

Incorporating viscous, toughness, and intermediate regimes of propagation into enhanced pseudo-3D model



Dontsov, E.V. and Peirce, A.P.

University of British Columbia, Vancouver, BC, Canada

Copyright 2015 ARMA, American Rock Mechanics Association

This paper was prepared for presentation at the 49th US Rock Mechanics / Geomechanics Symposium held in San Francisco, CA, USA, 28 June–1 July 2015.

This paper was selected for presentation at the symposium by an ARMA Technical Program Committee based on a technical and critical review of the paper by a minimum of two technical reviewers. The material, as presented, does not necessarily reflect any position of ARMA, its officers, or members. Electronic reproduction, distribution, or storage of any part of this paper for commercial purposes without the written consent of ARMA is prohibited. Permission to reproduce in print is restricted to an abstract of not more than 200 words; illustrations may not be copied. The abstract must contain conspicuous acknowledgement of where and by whom the paper was presented.

ABSTRACT: The design of a hydraulic fracturing treatment typically requires using a computational model that provides rapid results. One such possibility is to use the so-called classical pseudo-3D (P3D) model with symmetric stress barriers. Unfortunately, the original P3D model is unable to capture effects associated with fracture toughness in the lateral direction due to the fact that the assumption of plane-strain (or local) elasticity is used. On the other hand, a recently developed enhanced P3D model utilizes full elastic interactions and is capable of incorporating either toughness or viscous regimes of propagation by using the corresponding asymptotic solution at the tip element. Since either the viscous or toughness asymptote is used, the intermediate regime is not described accurately. To deal with this problem, this study aims to implement the intermediate asymptotic solution into the enhanced P3D model. To assess the level of accuracy, the results are compared to a reference solution. The latter reference solution is calculated numerically using a fully planar hydraulic fracturing simulator (Implicit Level Set Algorithm (ILSA)), which also incorporates the asymptotic solution for tip elements that captures the transition from viscous to toughness regime.

1. INTRODUCTION

Hydraulic fracturing (HF) plays a crucial role in the petroleum industry, as it allows one to perform reservoir stimulation and intensify hydrocarbon production [1]. To design a HF treatment, an appropriate HF model needs to be utilized. The simplest model is the one-dimensional Khristianovich-Zhel'tov-Geertsma-De Klerk (KGD) model [2], in which the fracture propagates in a plane, the elastic interactions are modelled assuming that plane strain conditions prevail, and the coupling between viscous fluid flow and elasticity is included. To represent the fracture geometry more realistically, the Perkins-Kern-Nordgren (PKN) model [3, 4] was developed to predict fracture propagation in a horizontally layered medium. The PKN model assumes that the fracture height is always equal to the thickness of the reservoir layer, the fracture opening in each vertical cross-section is taken to be elliptic, while the fluid pressure is calculated assuming that a plane strain condition holds in each cross-section. Given the fact that the PKN model does not allow for the height growth, the pseudo-3D (P3D) model, which permits height growth, has been developed [5]. Later, with

the increase of the computational power, more accurate planar 3D models (PL3D) were developed [7, 8]. As follows from the name, the fracture is contained in one plane, where the fracture geometry within this plane is discretized using a two-dimensional grid. Since the KGD, PKN and P3D are essentially one-dimensional models, while all varieties of PL3D are two-dimensional, the CPU time increases dramatically. The PL3D models improve accuracy and open the possibility of capturing different fracture geometries. Recently, researchers have shifted their effort to investigate the interaction between multiple hydraulic fractures that are growing simultaneously [9], and to describe non-planar fracture propagation [10].

Given the hierarchy of models described above, it is clear that recent more advanced models intend to capture more physical phenomena and thus represent real HF more accurately. At the same time, there are still situations when computational time imposes severe restrictions. In such situations, less accurate P3D models that are capable of producing rapid results are used. For instance, the P3D model is used in [11, 12] for production optimization purposes. Also, the interaction of multiple hydraulic frac-

tures is studied in [13] using a P3D modelling approach. For this reason, it is important to develop an accurate P3D model, which is capable of capturing as many physical phenomena as possible, but which is still able to produce results rapidly. To address this issue, an enhanced P3D model (EP3D) has been developed in [14]. This model introduces non-local elasticity and a correction for the viscous height growth, which together eliminate the two weakest points of the classical P3D model, namely: its inability to capture a viscous resistance in the height growth, and its inability to account for a fracture toughness in the lateral direction. As follows from [14], the EP3D model is able to accurately describe blade-like fractures that propagate either in the viscous or toughness regime, while the intermediate regime was not analyzed. To fill this gap, this study aims to incorporate the viscous-to-toughness propagation regime into the EP3D model and to compare the results to the fully planar HF simulator ILSA [15].

This paper is organized as follows. First, the EP3D model is briefly described in Section 2. Then, Section 3 outlines the asymptotic solution that is required to incorporate the viscous-to-toughness transition propagation regime into the EP3D model. After that, Section 4 presents the results of a comparison between the EP3D model and the fully planar ILSA simulator. Finally, Section 5 summarizes the results.

2. ENHANCED PSEUDO-3D (EP3D) MODEL

This section aims to briefly describe the EP3D model [14]. The EP3D model considers a fracture that propagates in a vertical plane, and is suppressed by two symmetric stress barriers located outside of the reservoir layer with thickness H , see Fig. 1. Key assumptions of the EP3D model include: i) uniform pressure over each vertical cross-section, and ii) fracture width variation in each vertical cross-section is approximated by the plane strain solution. For this study, it is also assumed that there is no leak-off.

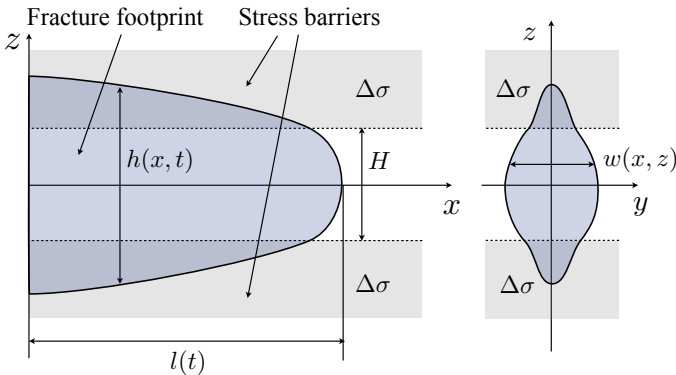


Figure 1: Schematics of an EP3D fracture.

With the aforementioned assumptions, the fracture

opening can be written as (see [16, 14])

$$w(x, z) = \frac{2}{E'} \sqrt{\frac{2}{\pi h}} K_{Ic} \chi + \frac{4\Delta\sigma}{\pi E'} \left\{ -z \ln \left| \frac{H\chi + 2z\psi}{H\chi - 2z\psi} \right| + \frac{H}{2} \ln \left| \frac{\chi + \psi}{\chi - \psi} \right| \right\}, \quad (1)$$

where $\chi = \sqrt{h^2 - 4z^2}$, $\psi = \sqrt{h^2 - H^2}$, $E' = E/(1 - \nu^2)$ is the plane strain Young's modulus, K_{Ic} is the fracture toughness, $\Delta\sigma$ is the magnitude of the stress barriers, H is the thickness of the reservoir layer, and h is the fracture height. Note that the x dependence in (1) comes from the variation of fracture height $h(x)$. The EP3D model can be effectively formulated in terms of the effective width, defined as

$$\bar{w} = \frac{1}{H} \int_{-h/2}^{h/2} w dz. \quad (2)$$

In this case, equation (1) can be integrated to obtain

$$\bar{w} = \frac{H}{E'} \left(\sqrt{\frac{\pi}{2H}} K_{Ic} \left(\frac{h}{H} \right)^{3/2} + \Delta\sigma \sqrt{\frac{h^2}{H^2} - 1} \right). \quad (3)$$

Relation (3) can be inverted to find $h(\bar{w})$, which allows us to find the fracture height (and consequently $w(x, z)$ through (1)) knowing $\bar{w}(x)$. It should be noted here that formulas (1) and (3) apply only in the regions with $h \geq H$, i.e. when there is height growth through the stress barriers. In situations when $h < H$, equations (1) and (3) are replaced with

$$w = \frac{4H}{\pi h^2} \bar{w} \chi, \quad \bar{w} = \sqrt{\frac{\pi}{2}} \frac{K_{Ic} h^2}{E' H (\min\{2l, H\})^{1/2}}, \quad (4)$$

where the latter is obtained using the analytic solution for a radial fracture propagating in the toughness regime. Here l is the fracture half-length and $\chi = \sqrt{h^2 - 4z^2}$ as defined earlier.

Given the fact that the pressure is uniform in each vertical cross-section, the lubrication equation can be integrated over the vertical coordinate to obtain

$$\frac{\partial \bar{w}}{\partial t} + \frac{\partial \bar{q}_x}{\partial x} = \frac{Q_0}{H} \delta(x), \quad (5)$$

where the averaged flux is given by

$$\bar{q}_x = -\frac{1}{H\mu'} \frac{\partial p}{\partial x} \int_{-h/2}^{h/2} w^3 dz, \quad (6)$$

Here Q_0 is the total fluid volume pumped into the fracture per unit time, $\mu' = 12\mu$, where μ is the fracturing fluid viscosity, and p is the fluid pressure.

To obtain the fluid pressure, the classical P3D model [16] uses the plane strain pressure, which is given by

$$p_{ps} = \Delta\sigma \left[1 + \sqrt{\frac{2}{\pi H}} \frac{K_{Ic}}{\Delta\sigma} \sqrt{\frac{H}{h}} - \frac{2}{\pi} \arcsin\left(\frac{H}{h}\right) \right]. \quad (7)$$

In contrast, EP3D utilizes non-local elasticity, for which the fluid pressure is given by

$$p(x) = -\frac{E'}{8\pi} \int_{-l(t)}^{l(t)} \int_{-\frac{1}{2}h(x',t)}^{\frac{1}{2}h(x',t)} \frac{w(x', z') dz' dx'}{((x'-x)^2 + z'^2)^{3/2}}, \quad (8)$$

where equation (1) is used to calculate fracture opening. A similar two-dimensional elasticity integral (8) is used in the fully planar 3D fracture simulator ILSA [8] to calculate fluid pressure. For the purpose of fast evaluation of the two-dimensional integral (8), the fracture opening in each vertical cross-section is approximated by two ellipses. Then, the integral over the vertical coordinate z' can be evaluated analytically. This procedure reduces the numerical evaluation of the two-dimensional integral to two one-dimensional integrals, and the whole problem becomes one-dimensional as well. See more details in [14].

The fracture opening (1) features the fracture toughness and clearly represents the solution corresponding to the toughness regime. In situations when the fracture toughness is small, or zero, this solution becomes inaccurate. To incorporate viscous height growth approximately using the toughness solution (1) an apparent toughness is introduced. This apparent toughness introduces a resistance that matches the corresponding resistance due to the viscous dissipation near the fracture tip. In this case, the apparent toughness mimics the viscous resistance in the vertical direction and controls the vertical height growth. More details can be found in [14].

To effectively solve the problem under consideration numerically, a scaled spatial coordinate is introduced as $x = l(t)\xi$, $0 \leq \xi \leq 1$. In this case equation (5) can be rewritten as

$$\frac{\partial \bar{w}}{\partial t} - \frac{V\xi}{l} \frac{\partial \bar{w}}{\partial \xi} + \frac{1}{l} \frac{\partial \bar{q}_x}{\partial \xi} = \frac{Q_0}{Hl} \delta(\xi), \quad (9)$$

where $V = dl/dt$ is the velocity of the fracture tip. In the numerical scheme, the spatial coordinate ξ is discretized using a uniform grid. Likewise, \bar{w} is defined on the set of discretized spatial points. Central differences are used to discretize the flux derivative in (9) and the pressure derivative in (6), the trapezoidal rule is used to evaluate the integral in (6), and a backward difference is used to approximate the time derivative in (9). It should also be noted that the fracture height and fracture opening are calculated using (3) and (1) or (4) for given values of \bar{w} . The displacement discontinuity method is used to calculate the pressure via an approximation of (8) (see the discussion above). Since the displacement discontinuity method does not give an accurate result for the tip element, the fluid pressure at the tip is treated as an unknown. To compensate for the introduction of the new degree of freedom, the fracture velocity V is calculated assuming that the solution at the tip follows the asymptotic solution for the

KGD fracture, see e.g. [8, 15]. In situations when there is no fracture toughness, the fracture velocity V is calculated using the viscous asymptotic solution

$$V = \frac{E'}{\mu' \beta_m^3 (l\Delta\xi)^2}, \quad (10)$$

where $\beta_m = 2^{1/3} \cdot 3^{5/6}$, $w(\Delta\xi)$ is the fracture opening at $z = 0$ for the penultimate node, and $l\Delta\xi$ is the distance between two nodes. In situations when the fracture toughness is significant, and the hydraulic fracture propagates in the toughness regime, the velocity is adjusted in a way that the toughness propagation criterion holds for the last element, namely

$$w(\Delta\xi) = \sqrt{\frac{32}{\pi}} \frac{K_{Ic}}{E'} \sqrt{l\Delta\xi}. \quad (11)$$

Once the tip velocity is calculated, the discretized nonlinear equation (9) is solved iteratively for \bar{w} . Then, using the same value of the tip velocity, the fracture length is updated.

As discussed in [14], the EP3D model described above shows good agreement with the reference ILSA solution in situations when the fracture propagates in either the viscous or the toughness regime. However, the original EP3D model switches between the viscous asymptotic solution (10) and the toughness asymptotic solution (11) for the intermediate regime. This leads to inaccuracies and non-smooth fracture growth in situations when the fracture propagates in the intermediate regime. To address this issue, this study aims to incorporate the viscous-to-toughness intermediate regime of propagation into the EP3D model. This will make EP3D model even more accurate, in which case the corresponding HF simulator can produce reliable and, at the same time, rapid results.

3. INCORPORATING VISCOUS-TO-TOUGHNESS INTERMEDIATE REGIME OF PROPAGATION

The asymptotic solutions used in (10) and (11) originate from the solution for the semi-infinite KGD fracture propagating with the velocity V and represent two limiting cases of no fracture toughness and no fluid viscosity. An intermediate regime of propagation for the semi-infinite fracture, where both fracture toughness and fluid viscosity affect the solution, is analyzed in [17]. The solution for the fracture opening of the semi-infinite KGD fracture propagating with the velocity V , written in dimensionless form, is given by

$$\hat{w} = \hat{\Omega}(\hat{\xi}). \quad (12)$$

Here the scaled fracture opening \hat{w} and the scaled spatial coordinate $\hat{\xi}$ are

$$\hat{w} = \frac{E'^3 \mu' V}{K'^4} w, \quad \hat{\xi} = \frac{E'^4 \mu'^2 V^2}{K'^6} s,$$

where w denotes fracture opening, s is the co-ordinate along the fracture that originates at the tip, $K' = \sqrt{32/\pi} K_{Ic}$ is the scaled fracture toughness, $E' = E/(1-\nu^2)$ is the plane strain Young's modulus, $\mu' = 12\mu$ is a scaled fluid viscosity, and V is the crack tip velocity. Fig. 2 shows the solution (12), calculated numerically in [17]. The function $\hat{\Omega}(\hat{\xi})$ has two asymptotes. In situations when $\hat{\xi}$ is small, $\hat{\Omega}(\hat{\xi}) \approx \hat{\xi}^{1/2}$, which corresponds to the toughness asymptote (11). Situations when $\hat{\xi}$ is large correspond to the viscous asymptote (10) and $\hat{\Omega}(\hat{\xi}) \approx \beta_m \hat{\xi}^{2/3}$.

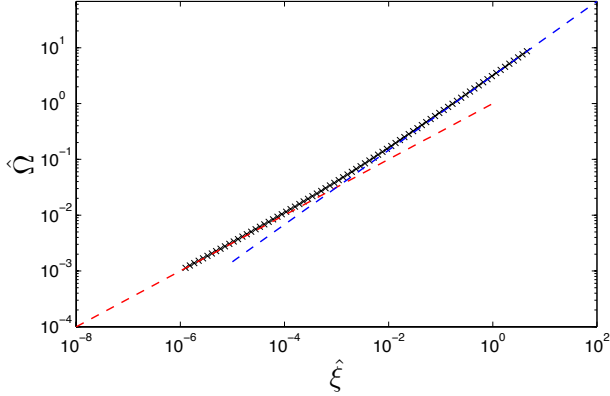


Figure 2: Function $\hat{\Omega}(\hat{\xi})$ (12) calculated numerically (markers) and the two asymptotes, namely, $\hat{\Omega}(\hat{\xi}) = \hat{\xi}^{1/2}$ for $\hat{\xi} \rightarrow 0$ (dashed red line) and $\hat{\Omega}(\hat{\xi}) = \beta_m \hat{\xi}^{2/3}$ for $\hat{\xi} \rightarrow \infty$ (dashed blue line).

To be able to find the velocity of propagation for a given fracture width and the distance from the tip, it is useful to introduce a different scaling, so that

$$\hat{K} = \frac{K' s^{1/2}}{E' w}, \quad \hat{V} = \frac{\mu'}{E'} \frac{\beta_m^3 s^2}{w^3} V.$$

in which case (12) can be rewritten as

$$\frac{\hat{V}}{\beta_m^3 \hat{K}^4} = \hat{\Omega} \left(\frac{\hat{V}^2}{\beta_m^6 \hat{K}^6} \right). \quad (13)$$

By introducing the function $\bar{\Omega}(\hat{\xi}) = \hat{\xi}^{-1/2} \hat{\Omega}(\hat{\xi})$, equation (13) can be solved for \hat{V} as

$$\hat{V} = \beta_m^3 \hat{K}^3 \sqrt{\bar{\Omega}^{-1}((\hat{K})^{-1})} = \hat{V}_{MK}(\hat{K}). \quad (14)$$

One possibility to calculate the scaled fracture velocity \hat{V} is to precompute the function $V_{MK}(\hat{K})$ and use it to evaluate \hat{V} . However, since the EP3D model already utilizes multiple approximations aimed to increase computational efficiency, we are going to introduce an approximation for the function $\hat{V}_{MK}(\hat{K})$ in (14) as well. To this end, let us approximate $\hat{V}_{MK}(\hat{K})$ by

$$\hat{V}_{MK}(\hat{K}) \approx \frac{1 - \hat{K}^{p_1}}{1 + p_2 \hat{K}^{p_1}}, \quad (15)$$

where p_1 and p_2 are two parameters. By minimizing the L^2 error between the numerically calculated $\hat{V}_{MK}(\hat{K})$ and the approximation (15), it is found that $p_1 = 3.0077$ and $p_2 = 0.1572$ correspond to the minimum L^2 error whose magnitude is $O(10^{-3})$. Note that the clues to the functional form of (15) are obtained by analyzing the asymptotic behaviour of $\hat{V}_{MK}(\hat{K})$ at $\hat{K} \approx 0$ (which corresponds to the viscous regime) and $\hat{K} \approx 1$ (which corresponds to the toughness regime), which is performed by including the second order terms in the asymptotic expansion of $\hat{\Omega}(\hat{\xi})$ for $\hat{\xi} \rightarrow 0$ and $\hat{\xi} \rightarrow \infty$, see [15]. For completeness, it is noted that $\hat{K} > 1$ corresponds to the case when the stress intensity factor is smaller than K_{Ic} , in which case the fracture does not propagate. In this situation, (15) should be complemented by $\hat{V}_{MK}(\hat{K}) = 0$ for $\hat{K} > 1$. As an illustration, Fig. 3 plots the numerically calculated $\hat{V}_{MK}(\hat{K})$ (markers) and the approximation given by (15) (solid line).

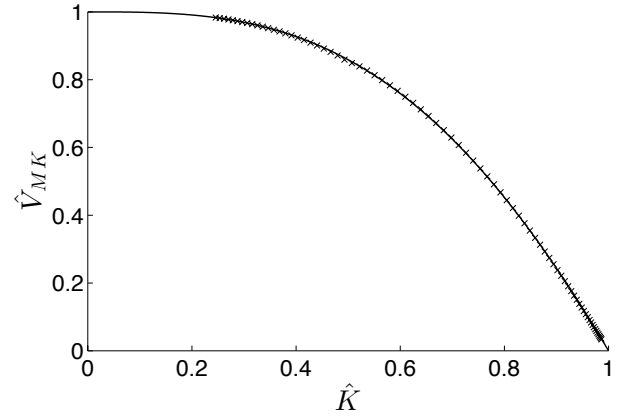


Figure 3: Variation of the function $\hat{V}_{MK}(\hat{K})$ (14) calculated numerically (markers) and the approximation given by (15) (solid line).

Finally, to implement the intermediate propagation regime into the EP3D HF simulator, one needs to replace the subroutine for calculating the fracture velocity (see equations (10) and (11)) with the following expression

$$V = V_M \max \left\{ \frac{1 - \hat{K}^{p_1}}{1 + p_2 \hat{K}^{p_1}}, 0 \right\}. \quad (16)$$

Here V_M represents the velocity that correspond to the viscous solution, while \hat{K} is scaled fracture toughness, namely

$$V_M = \frac{E'}{\mu'} \frac{w(\Delta\xi)^3}{\beta_m^3 (l\Delta\xi)^2}, \quad \hat{K} = \frac{K'(l\Delta\xi)^{1/2}}{E'w(\Delta\xi)}.$$

As before, $w(\Delta\xi)$ denotes the fracture opening of the penultimate element, and $l\Delta\xi$ is the distance between neighbouring elements.

4. RESULTS AND DISCUSSION

This section compares the results obtained using the EP3D model with the intermediate (or MK) asymptotic solution described in the previous section to the reference solution. The reference solution is obtained using the Implicit Level Set Algorithm (ILSA) scheme [8, 15]. The parameters for the computation are chosen as $H = 0.05$ m, $\mu = 30.2$ Pa·s, $\nu = 0.4$, $E = 3.3$ GPa, $Q_0 = 1.7$ mm³/s, $\Delta\sigma = 4.3$ MPa. The rock is assumed impermeable in both models (i.e. no leak-off). Different values of fracture toughness are considered. Fig. 4 compares the footprints obtained using ILSA and EP3D for $K' = 0$ (blue lines), $K' = 1.75$ MPa·m^{1/2} (magenta lines), and $K' = 3.0$ MPa·m^{1/2} (red lines) at different time instants $t = 200$ s, $t = 401$ s, and $t = 604$ s. Note that $K' = \sqrt{32/\pi} K_{IC}$. As can be seen from the figure, the EP3D model is capable of approximating the reference ILSA solution accurately for different values of fracture toughness. It is important to note that $\hat{\xi} \approx 3 \times 10^{-5}$ and $\hat{K} \approx 0.94$ for $K' = 1.75$ MPa·m^{1/2}, which corresponds to the intermediate regime (see discussion about regimes classification below). Curves with $K' = 3.0$ MPa·m^{1/2} correspond to the toughness regime with $\hat{\xi} \approx 5.5 \times 10^{-7}$ and $\hat{K} \approx 0.99$. While data with $K' = 0$ corresponds to the viscous regime with $\hat{\xi} = \infty$ and $\hat{K} = 0$.

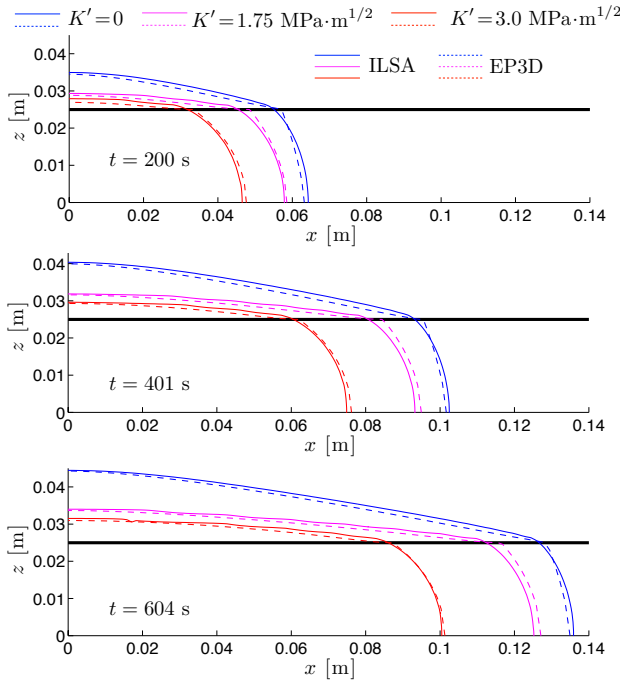


Figure 4: Comparison between fracture footprints calculated using the EP3D and ILSA simulators for different values of fracture toughness sampled at different time instants.

To quantify the effect of the appropriate asymptotic solution on the accuracy, Fig. 5 compares the half-lengths l calculated using ILSA and EP3D at $t = 604$ s for different values of the fracture toughness K' . The blue markers

represent the original EP3D model, where the simulator used a switch between viscous and toughness asymptotic solutions, while the red markers correspond to the EP3D model for which intermediate asymptotic solution is used. Fig. 5 shows that the intermediate asymptote noticeably affects the solution when $1.25 < K' < 2.5$. This corresponds to $2.6 \times 10^{-6} < \hat{\xi} < 2.7 \times 10^{-4}$ and $0.86 < \hat{K} < 0.98$. This result is somewhat counterintuitive, because Figs. 2 and 3 show that the transition zone should approximately be $10^{-4} < \hat{\xi} < 10^{-2}$ and $0.4 < \hat{K} < 0.8$. One possible explanation is that V_M in (16) is proportional to the cube of the fracture width. In this situation, even moderate variations of \hat{V}_{MK} can be compensated by relatively small changes of the fracture width. However, when \hat{V}_{MK} becomes small, the effect becomes more pronounced and the transition regime occurs. To support this hypothesis, it is noted that the values $0.86 < \hat{K} < 0.98$ correspond to $0.37 < (\hat{V}_{MK})^{1/3} < 0.7$. In this case, it is convenient to identify the intermediate regime by the values of $(\hat{V}_{MK})^{1/3}$. Small values of $(\hat{V}_{MK})^{1/3}$ correspond to the toughness regime, values that are $(\hat{V}_{MK})^{1/3} \approx 0.5$ correspond to the intermediate regime, while values of $(\hat{V}_{MK})^{1/3}$ that are close to one represent the viscous regime of propagation. Note that $\hat{K} \approx 0.94$ corresponds to $(\hat{V}_{MK})^{1/3} = 0.53$, which, according to the adopted definition, corresponds to the intermediate regime. Fig. 5 also shows that the use of the appropriate asymptotic solution decreases the discrepancy with the reference solution by more than a factor of two. In addition to that, the use of the MK asymptote does not affect the computational time, and produces smoother fracture growth through the transition zone. It should also be noted that the discrepancy between EP3D and ILSA results does not vanish for the viscous and toughness regimes because the EP3D model utilizes multiple approximations, that affect overall accuracy, but, at the same time, drastically increase the computational efficiency.

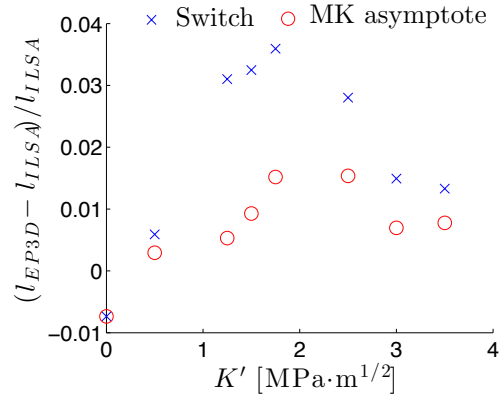


Figure 5: Fracture length discrepancy between EP3D and ILSA results for $t = 604$ s versus K' . Blue markers correspond to the EP3D which switches between viscous and toughness asymptotic solutions, while red markers represent results of the EP3D that uses the MK asymptote.

5. SUMMARY

The goal of this study is to augment EP3D model with the viscous-to-toughness asymptotic solution, which increases the accuracy of the model predictions in the transition regime. Firstly, the EP3D model, which accounts for non-local elasticity and viscous height growth (no leak-off), is briefly described. Since the EP3D model utilizes the asymptotic solution for the tip element to determine fracture propagation velocity, it is necessary to include the appropriate asymptotic solution. In particular, this asymptotic solution captures the transition from the viscous to the toughness regime of propagation. To increase the computational efficiency, the fracture velocity, that is calculated numerically using the asymptotic solution, is approximated by an analytical formula. It is shown that the error induced by the approximation is $O(10^{-3})$. The predictions of the EP3D model with the new asymptotic solution are compared to the reference ILSA solution, where the latter is a fully planar HF simulator. It is shown that the fracture footprints agree well for a range of values of fracture toughness, which represent: the viscous, toughness, and intermediate regimes of propagation. Finally, it is also shown that the use of the appropriate asymptotic solution decreases the discrepancy between the EP3D and ILSA results by more than a factor of two, and, at the same time, does not affect the computational efficiency of the EP3D model.

REFERENCES

1. Economides, M.J. and K.G. Nolte, editors. 2000. *Reservoir Stimulation*. John Wiley & Sons, Chichester, UK, 3rd edition.
2. Khristianovic, S.A. and Y.P. Zheltov. 1955. Formation of vertical fractures by means of highly viscous fluids. *In Proc. 4th World Petroleum Congress*, 2:579–586.
3. Perkins, T.K. and L.R. Kern. 1961. Widths of hydraulic fractures. *In J. Pet. Tech. Trans. AIME*, 937–949.
4. Nordgren, R.P. 1972. Propagation of vertical hydraulic fractures. *In J. Pet. Technol.*, 306–314.
5. Palmer, I.D. and H.B. Carroll. 1982. Three-dimensional hydraulic fracture propagation in the presence of stress variation. *In Proceedings of the SPE/DOE/GRI unconventional gas recovery symposium, SPE/DOE 10849.*, 870–878.
6. Settari, A. and M.P. Cleary. 1982. Development and testing of a pseudo-three-dimensional model of hydraulic fracture geometry (p3dh). *In Proceedings of the 6th SPE symposium on reservoir simulation of the Society of Petroleum Engineers, SPE 10505.*, 185–214.
7. Advani, S. H., T.S. Lee and J.K. Lee. 1990. Three-dimensional modeling of hydraulic fractures in layered media: Part I-finite element formulations. *J. Energy Resour. Technol.*, 112:1–9.
8. Peirce, A. and E. Detournay. 2008. An implicit level set method for modeling hydraulically driven fractures. *Comput. Methods Appl. Mech. Engrg.*, 197:2858–2885.
9. Peirce, A. and A.P. Bungler. 2014. Interference fracturing: Non-uniform distributions of perforation clusters that promote simultaneous growth of multiple hydraulic fractures. *SPE 172500*.
10. Napier, J. A. L. and E. Detournay. 2013. Propagation of non-planar pressurized cracks from a borehole. *In Research and Applications in Structural Engineering, Mechanics and Computation*, 597–602.
11. Yang, M. 2012. Hydraulic fracture production optimization with a pseudo-3D model in multilayered lithology. *In Society of Petroleum Engineers, SPE 149833*.
12. Kordziel, W.R., W. Rowe, V.B. Dolan, and S.D. Ritger. 1996. A case study of integrating well-logs and a pseudo 3D multi-layer frac model to optimize exploitation of tight lenticular gas sands. *In Society of Petroleum Engineers, SPE 36866*.
13. Wu, R., O. Kresse, X. Weng, C.-E. Cohen, and H. Gu. 2012. Modeling of interaction of hydraulic fractures in complex fracture networks. *In Society of Petroleum Engineers, SPE 152052*.
14. Dontsov, E. and A. Peirce. 2015. An enhanced pseudo-3D model for hydraulic fracturing accounting for viscous height growth, non-local elasticity, and lateral toughness. <http://hdl.handle.net/2429/52289>.
15. Peirce, A.P. 2015. Modeling multi-scale processes in hydraulic fracture propagation using the implicit level set algorithm. *Comp. Meth. in Appl. Mech. and Eng.*, 283:881–908.
16. Adachi, J.I., E. Detournay, and A.P. Peirce. 2010. An analysis of classical pseudo-3D model for hydraulic fracture with equilibrium height growth across stress barriers. *Int. J. of Rock Mech. and Min. Sci.*, 47:625–639.
17. Garagash, D.I. and E. Detournay. 2000. The tip region of a fluid-driven fracture in an elastic medium. *ASME J. Appl. Mech.*, 67:183–192.